**Supporting Information**

for

# Partially Oxidized $Ti_3C_2T_x$ MXenes for Fast and Selective Detection of Organic Vapors at Part-per-Million Concentrations

Hanna Pazniak, [*,†] Ilya A. Plugin, [‡] Michael J. Loes, [△] Talgat M. Inerbaev, [§,⊥] Igor N. Burmistrov, [†,|] Michail Gorshenkov, [†] Josef Polcak, [#,‖] Alexey S. Varezhnikov, [‡] Martin Sommer, [▽] Denis V. Kuznetsov, [†] Michael Bruns, [°] Fedor S. Fedorov, [+] Nataliia S. Vorobeva, [△] Alexander Sinitskii, [*,△] Victor V. Sysoev [*,‡]

[†]Department of Functional Nanosystems and High-Temperature Materials, National University of Science and Technology "MISiS", Moscow, 119049, Russia

[‡]Department of Physics, Yuri Gagarin State Technical University of Saratov, Saratov, 410054, Russia

[§]V. S. Sobolev Institute of Geology and Mineralogy SB RAS, Novosibirsk, 630090, Russia

[⊥]L. N. Gumilyov Eurasian National University, Astana, 010008, Kazakhstan

[|]Engineering Center, Department of Chemistry of Innovative Materials and Technologies

Plekhanov Russian University of Economics, Moscow, 117997, Russia

[#]CEITEC-Central European Institute of Technology, Brno University of Technology, Brno, 61600, Czech Republic

[‖]Institute of Physical Engineering, Brno University of Technology, Brno, 61669, Czech Republic

[▽]Institute of Microstructure Technology, Karlsruhe Institute of Technology, Eggenstein-Leopoldshafen, 76344, Germany

[°]Institute for Applied Materials, Karlsruhe Institute of Technology (KIT), Eggenstein-Leopoldshafen, 76344, Germany

[+]Skolkovo Institute of Science and Technology, Moscow, 121205, Russia

[△]Department of Chemistry, University of Nebraska-Lincoln, Lincoln, Nebraska 68588, United States

[*]*Email: hanna.pazniak@univ-poitiers.fr (H.P.), sinitskii@unl.edu (A.S.), vsysoev@sstu.ru (V.V.S).*

## Supporting Figures

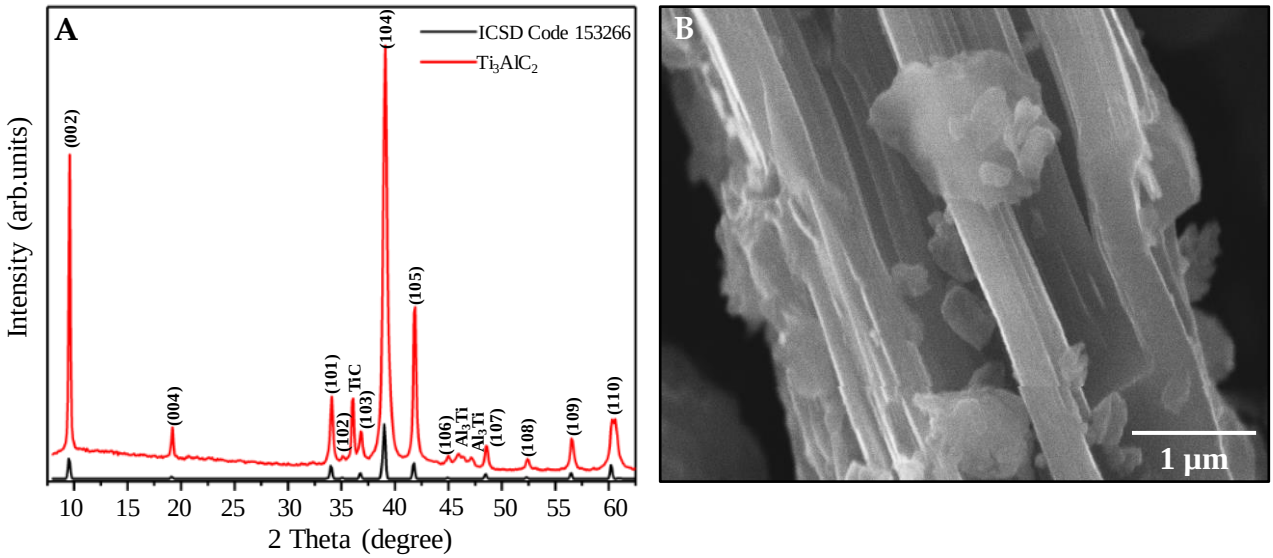


**Figure S1.** MAX phase characterization. (A) XRD pattern and (B) SEM image of $Ti_3AlC_2$ MAX phase powder used as a precursor for the MXene synthesis. The XRD pattern shows peaks corresponding to $Ti_3AlC_2$ (ICSD 153266); only small amounts of TiC and $Al_3Ti$ are identified as by-product phases. SEM image of $Ti_3AlC_2$ demonstrates a compact layered structure of particles that are typical for MAX phases

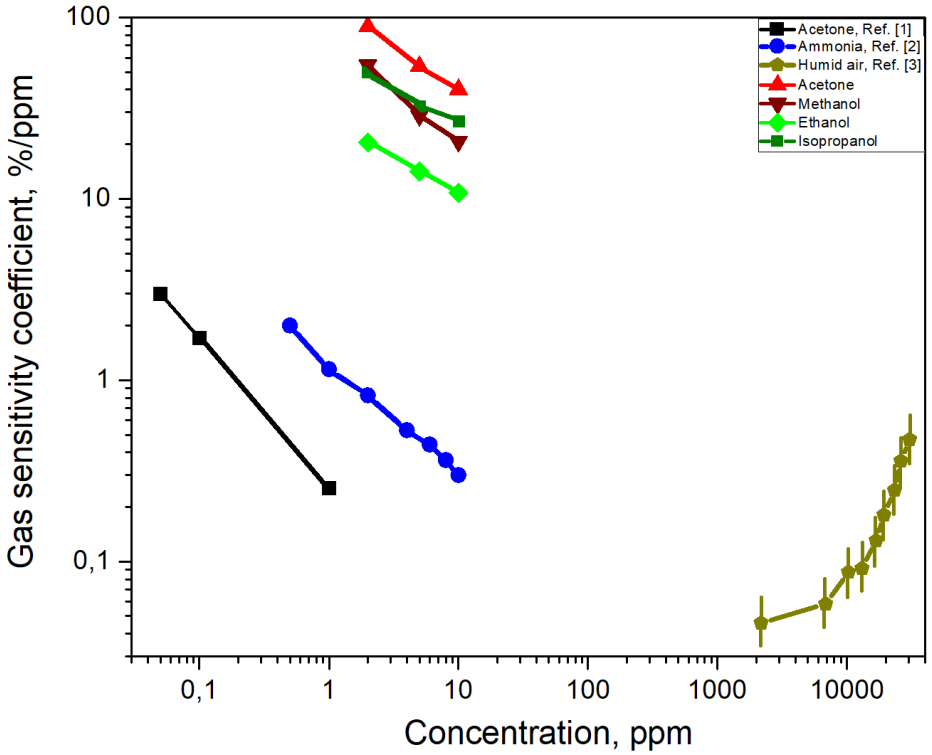


**Figure S2.** Comparison of gas response data obtained in this work *versus* the results reported in literature on the MXene-based structures.

Ref. [1] *ACS Nano*, **2018,** *12*, 986-993: Kim S.-J. et al. Metallic $Ti_3C_2T_x$ MXene Gas Sensors with Ultrahigh Signal-to-Noise Ratio;

Ref. [2] *Sensors and Actuators B*, **2019**, *298*, 126874: Tai, H. et al. "Enhanced ammonia response of $Ti_3C_2T_x$ nanosheets supported by $TiO_2$ nanoparticles at room temperature";

Ref. [3] *ACS Applied Materials & Interfaces*, **2019**, in press: Li N. et al. "High Performance Humidity Sensor Based on Urchin-like Composite of $Ti_3C_2$ MXene-derived $TiO_2$ Nanowires".

The gas sensitivity coefficient is calculated as $\alpha=S/K$ where $S=\Delta G/G_{air}$, $K$ is the gas concentration in ppm, $\Delta G$ is the sensor conductance change due to the gas exposure and $G_{air}$ is the sensor conductance in pure air. In case of data published in Ref. [3], $S=\Delta C/C_{air}$ where $\Delta C$ and $C_{air}$ are the sensor capacitance change due to the gas exposure and the capacitance in pure air, respectively. The data acquired from Ref. [3] are delivered for 20-30 $^{o}$C range because the authors have not reported the exact temperature under "room temperature" conditions

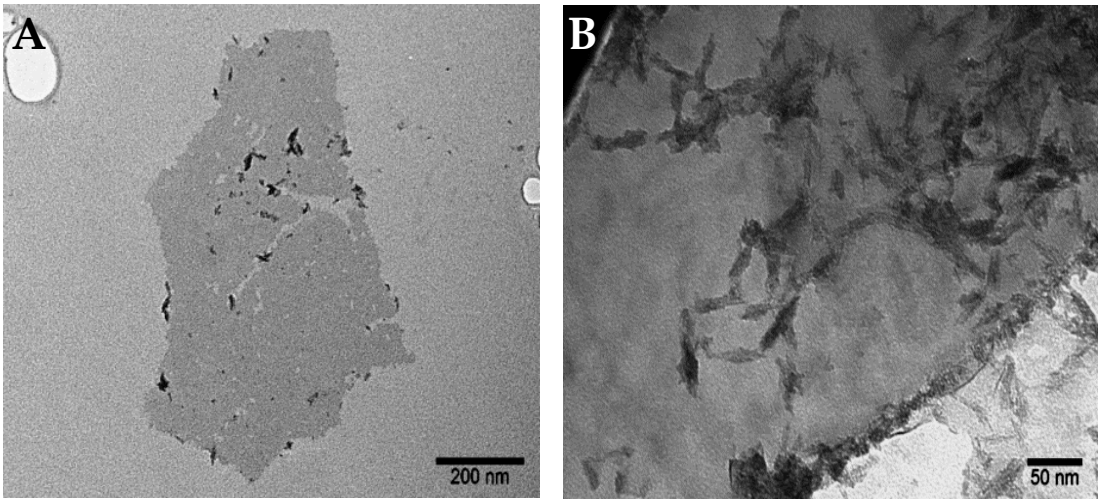


**Figure S3.** TEM image of MXene flake before (A) and after oxidation (B). MXenes flakes are atomically thin with irregular shapes and sizes. We observed the presence of a few tiny black impurities predominantly at the edges of flakes before the oxidation which are attributed to titanium dioxide. After the oxidation, almost the entire surface of flakes is covered with elongated particles

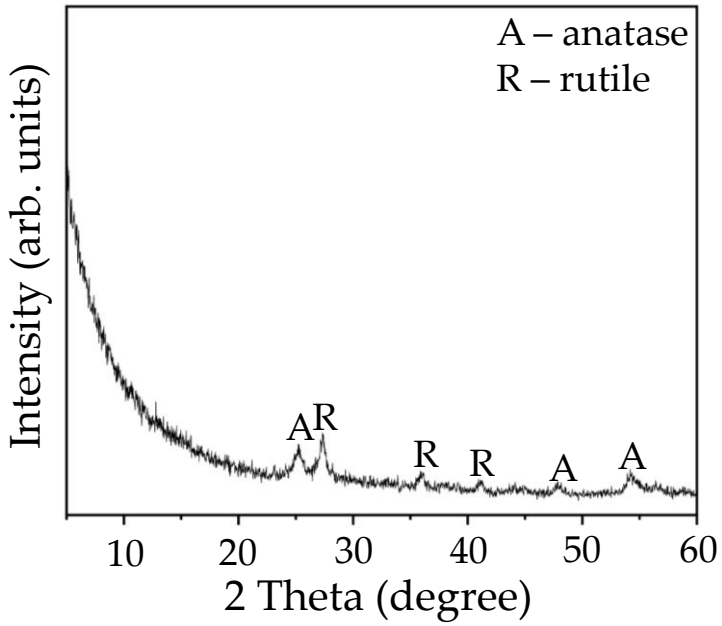


**Figure S4.** XRD pattern of MXene flakes after the oxidation at 600 ˚C in air

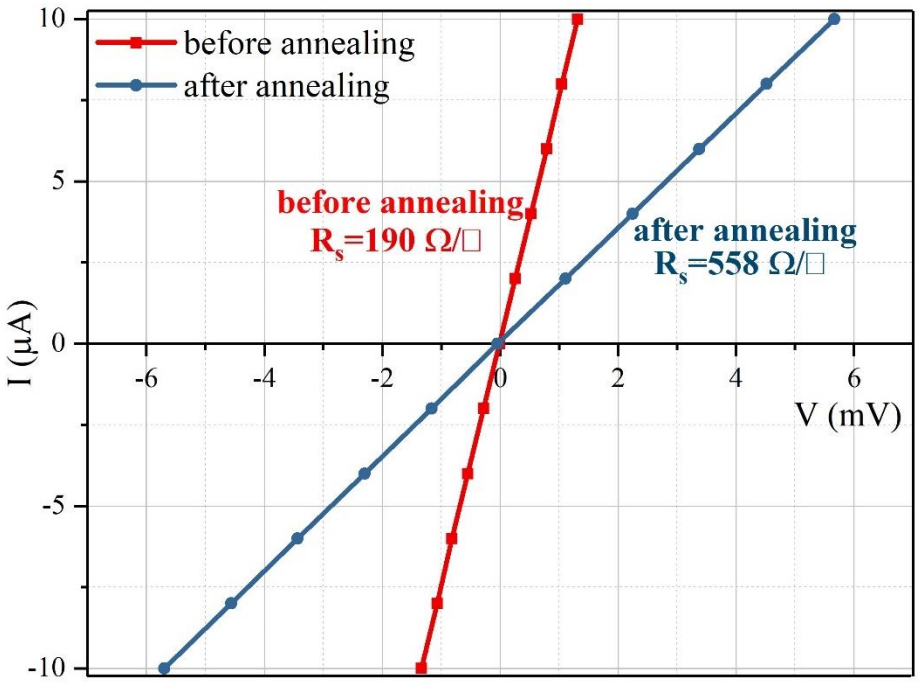


**Figure S5.** I-V dependence for the MXene film before and after annealing in air at 350 ˚C

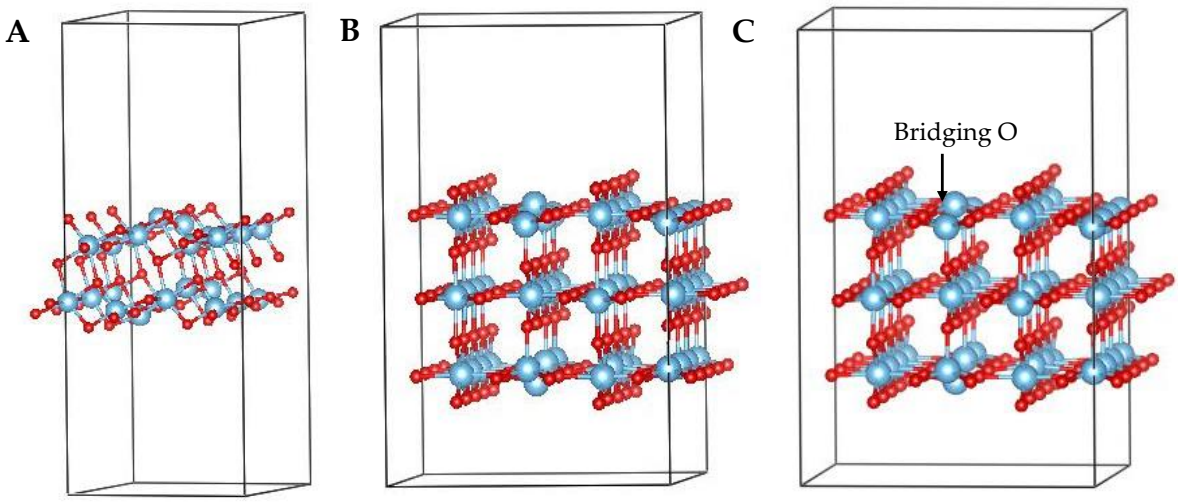


**Figure S6.** (A) (101) and (B), (C) (110) surface slabs of anatase and rutile structures, respectively. Blue circles are titanium atoms, small red circles are the oxygen atoms. The most prominent feature on rutile (110) surface is the presence of low-coordinated oxygen in the outermost layer. These oxygen atoms are referred to as bridging oxygens (Fig. C). They can be easily removed to introduce defects on a surface[S1]

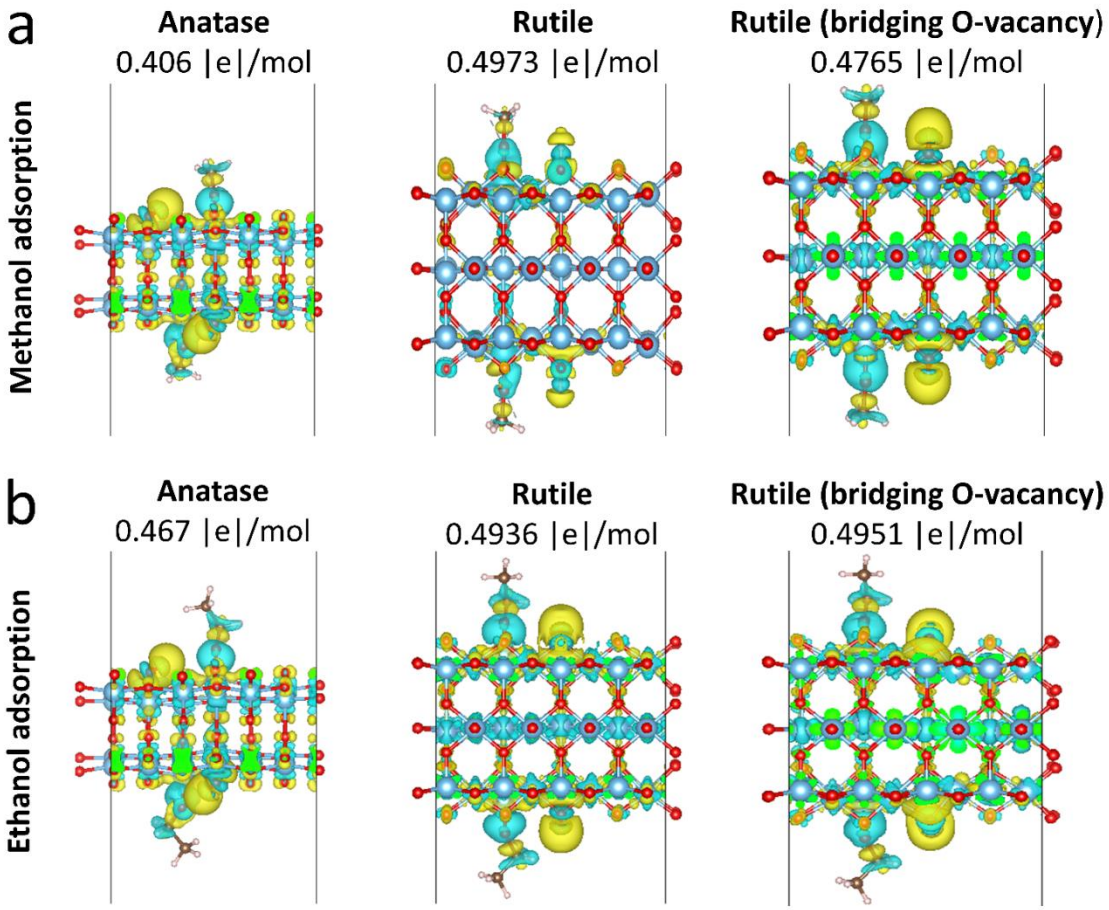


**Figure S7.** Electron density distributions in $TiO_2$ of various phases under adsorption of alcohol molecules: (a) case of methanol, (b) case of ethanol

We have concerned here only the alcohol molecules because acetone is known to thermally decompose[S2] and its further interaction with OH-groups on the MXenes surface results in the formation of two methanol molecules[S3]:

$$CH_3COCH_3 = CO + 2CH_3\cdot$$

$$2CH_3\cdot + OH^- = 2CH_3OH$$

DFT calculations were performed with Vienna Ab-Initio Simulation Package (VASP)[S3,S4] using the projector augmented-wave method[S5]. For the exchange and correlation functional we used the Perdew−Burke−Ernzerhof (PBE) version of the generalized gradient approximation[S6]. The van der Waals interactions were calculated using the Grimme DFT-D3 approach[S7]. The plane-wave basis energy cutoff was equal to 600 eV. The 4×4×1 Γ-centered k-point mesh and a denser 8×8×1 k-mesh were employed for the geometry optimization and calculation of electronic structure, respectively. A geometry relaxation was performed using the conjugated gradient method. The effective atomic charges are calculated using the Bader (topological) analysis[S8,S9].

## Supporting Table

**Table S1.** XPS peak fitting results for as-prepared and oxidized MXenes. The numbers in round brackets in column 2 are Ti $2p_{1/2}$ peak energies

| Region | Binding energy, eV | Assigned to | Fraction, % |
|---|---|---|---|
| **As-prepared MXene** | | | |
| Ti $2p_{3/2}$ ($2p_{1/2}$) | 455.1 (461.3) | Ti-C | 26.0 |
| | 455.8 (461.6) | Ti(II) | 22.3 |
| | 457.1 (462.9) | Ti(III) | 33.7 |
| | 458.9 (464.2) | $TiO_2$ | 18.0 |
| O 1s | 530.0 | $TiO_2$ | 28.9 |
| | 531.9 | C-Ti-$(OH)_x$ | 40.2 |
| | 533.5 | $H_2O_{ads}$ | 21.2 |
| | 535.4 | $Al(OF)_x$ | 9.7 |
| C 1s | 282.0 | Ti-C | 25.6 |
| | 285.0 | C-C/$CH_x$ | 61.3 |
| | 286.3 | C-O | 9.1 |
| | 289.1 | COO | 4.0 |
| **Oxidized MXene** | | | |
| Ti $2p_{3/2}$ ($2p_{1/2}$) | 455.0 (461.2) | Ti-C | 8.7 |
| | 457.2 (462.9) | Ti(III) | 5.4 |
| | 458.9 (464.5) | $TiO_2$ | 85.9 |
| O 1s | 530.2 | $TiO_2$ | 79.3 |
| | 531.9 | C-Ti-(OH)x | 20.7 |
| C 1s | 282.0 | Ti-C | 6.6 |
| | 285.0 | C-C/$CH_x$ | 84.8 |
| | 289.1 | COO | 8.6 |

## References


S1 Diebold, U.; Lehman, J.; Mahmoud, T.; Kuhn, M.; Leonardelli, G.; Hebenstreit, W.; Schmid, M.; Varga, P. Intrinsic Defects on a $TiO_2$(110)(1x1) Surface and Their Reaction With Oxygen: A Scanning Tunneling Microscopy Study. *Surf. Sci.* **1998**, *411*, 137.

S2 Sivaramakrishnan, R.; Su, M. C.; Michael, J. V.; Klippenstein, S. J.; Harding, L. B.; Ruscic, B. Rate Constants for the Thermal Decomposition of Ethanol and Its Bimolecular Reactions with OH and D: Reflected Shock Tube and Theoretical Studies. *J. Phys. Chem. A* **2010**, *114*, 9425-9439.

S3 Kresse, G.; Hafner, J. Ab initio Molecular Dynamics for Liquid Metals. *Phys. Rev. B* **1993**, *47*, 558-561.

S4 Kresse, G.; Furthmüller, J. Efficient Iterative Schemes for ab initio Total-Energy Calculations Using a Plane-Wave Basis Set. *Phys. Rev. B* **1996**, *54*, 11169-11186.

S5 Blöchl, P.E. Projector Augmented-Wave Method. *Phys. Rev. B* **1994**, *50*, 7953-17979.

S6 Li, S.; Zou, X.; Hu, Y.; Lu, X.; Xiong, X.; Xu, Q.; Cheng, H.; Zhou, Z. Electrosynthesis of Two-Dimensional TiC and C Materials from $Ti_3SiC_2$ in Molten Salt. *J. Electrochem. Soc.* **2018**, *165*, 190-195.

S7 Grimme, S.; Antony, J.; Ehrlich, S.; Krieg, H. A Consistent and Accurate ab initio Parametrization of Density Functional Dispersion Correction (DFT-D) for the 94 Elements H-Pu. *J. Phys. Chem.* **2010**, *132*, 154104.

S8 Muñoz, D.; Harrison, N. M.; Illas, F. Electronic and Magnetic Structure of $LaMnO_3$ From Hybrid Periodic Density-Functional Theory. *Phys. Rev. B* **2004**, *69*, 085115.

S9 Henkelman, G.; Arnaldsson, A.; Jónsson, H. A Fast and Robust Algorithm for Bader Decomposition of Charge Density. *Computational Materials Science* **2006**, *36*, 354-360.